The Organometallic Route to Highly Coherent Molecular Spin Qubits

Luana C. de Camargo,[§] Matteo Briganti,[§] Francielli S. Santana, Danilo Stinghen, Ronny R. Ribeiro, Giovana G. Nunes, Jaísa F. Soares,* Enrico Salvadori, Mario Chiesa,* Stefano Benci, Renato Torre, Lorenzo Sorace, Federico Totti, and Roberta Sessoli*

Dr. M. Briganti, Prof. L. Sorace, Prof. F. Totti, Prof. R. Sessoli
Department of Chemistry "U. Schiff" and INSTM UdR Firenze, University of Florence
Via della Lastruccia 3-13, 50019 Sesto Fiorentino, Italy
E-mail: Roberta.sessoli@unifi.it

L. C. de Camargo, F. S. Santana, Dr. M. Briganti, Dr. D. Stinghen, Prof. R. R. Ribeiro, Prof. G. G. Nunes, Prof. J. F. Soares
Department of Chemistry, Federal University of Parana
Centro Politecnico, Jardim das Americas, 81530-900 Curitiba-PR, Brazil
E-mail: jaisa@quimica.ufpr.br

Dr. E. Salvadori, Prof. M. Chiesa
Department of Chemistry, University of Turin
Via Giuria 7, 10125 Torino, Italy
E-mail: mario.chiesa@unito.it

S. Benci, Prof. R. Torre
Laboratory for Nonlinear Spectroscopy, University of Florence, Via Nello Carrara 1, 50019 Sesto Fiorentino, Italy

Prof. R. Torre
Department of Physics and Astrophysics, University of Florence, Via G.Sansone 1, 50019 Sesto Fiorentino, Italy

Prof. R. Sessoli
ICCOM-CNR, via Madonna del Piano 10, 50019 Sesto Fiorentino, Italy

§ These authors contributed equally

Abstract: The coherence time of the 17-electron, mixed sandwich complex [CpTi(cot)], (η^8-cyclooctatetraene)(η^5-cyclopentadienyl)- titanium, was found to reach 34 μs at 4.5 K in a frozen deuterated toluene solution. This result represents a remarkable coherence time for a highly protonated molecule. We here confirm that the intramolecular distances between the Ti and H atoms provide a good compromise between instantaneous and spin diffusion sources of decoherence. In addition, *ab initio* calculations at the molecular and crystal packing levels reveal that the characteristic low-energy ring rotations of the sandwich framework do not yield a detrimental spin-lattice relaxation because of their small spin-phonon coupling. Much shorter and almost temperature-independent phase memory times T_m were observed when [CpTi(cot)] was diluted in the diamagnetic (16-electron) crystalline host [CpTi(cht)], (η^7-cycloheptatrienyl)(η^5-cyclopentadienyl)titanium. Such finding reinforces the deactivating role of both intermolecular interactions involving the hydrogen atoms of neighboring molecules and cluster formation in the host crystal lattice. The volatility of [CpTi(cot)] and the accessibility of the semi-occupied, non-bonding d_{z^2} orbital make this neutral compound an ideal candidate for single-qubit addressing on surface and quantum sensing in combination with scanning probe microscopies.

Organometallic sandwich complexes of paramagnetic lanthanide ions are currently the focus of great interest because of the observation that dysprosium(III) derivatives present magnetic hysteresis of molecular origin, i.e. Single-Molecule Magnet (SMM) behavior, above liquid nitrogen temperature.[1] This outstanding performance results from a strongly axial crystal field. Equally relevant to the slow relaxation of the magnetization is the reduced spin–phonon coupling of the metal–ligand vibrational modes given the delocalized electron density on the cyclopentadienyl ligands.[1a,2] Concerning 3d metal ions, ferrocinium complexes only show slow relaxation of the magnetization in applied static fields.[3] Remarkably, the neutral nickelocene complex, bis(η^5-cyclopentadienyl)nickel, characterized by the spin state S=1 with easy plane anisotropy, has revealed an outstanding capability to act as a local magnetic sensor when adsorbed on the tip of a scanning tunnel microscope.[4]

Alternatively, sandwich complexes of early-transition metal ions such as Ti and V carrying one unpaired electron are also well known, but, to the best of our knowledge, their spin dynamics have not been reported. In our search for highly coherent, evaporable magnetic molecules as potential molecular spin qubits and sensors,[5] we identified in [CpTi(cot)] (**1** in Figure 1, left),

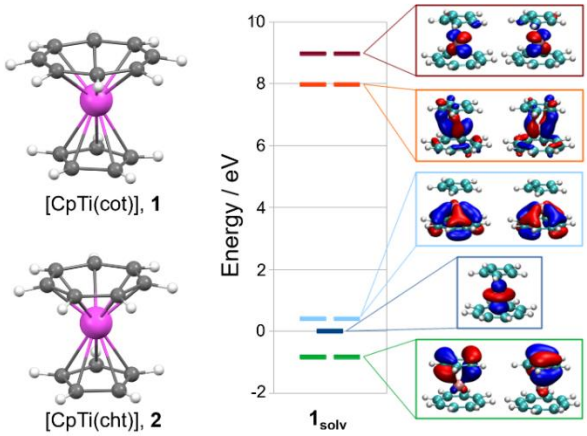

where Cp = η^5-C_5H_5 and cot = η^8-C_8H_8 are formally treated as mono- and di-anions respectively, a promising S=1/2 candidate. Starting from the synthesis,[6] crystal structure,[7] continuous-wave (CW) EPR,[8] and ENDOR[9] spectra reported a few decades ago, we here revisit and update relevant data on **1** that are of interest to the state-of-art of molecular qubit studies. Moreover, we report a pulsed EPR investigation combined with *ab initio* calculations to confirm the unique electronic and vibrational properties of this class of molecules as highly beneficial to boost coherence time in S=1/2 molecules. We found that despite the very low energy of the rotational mode of the rings and the presence of many hydrogen atoms in the ligands, coherence time in frozen solution reaches the remarkable value of tens of μs. The long coherence, coupled with the peculiar features of frontier orbitals that are very relevant for sensing properties,[4a,4b] makes this molecule extremely appealing for applications in quantum nanoscience.

Figure 1. Left: Molecular structure of the paramagnetic [CpTi(cot)] and diamagnetic [CpTi(cht)] complexes; Right: Energies and wave-functions of the molecular orbitals of [CpTi(cot)] (spin α) in the presence of implicit toluene solvent, computed by the Conductor-like Polarizable Continuum Model.

Synthesis of **1** was performed by a new and accessible route that comprises reaction of [Cp_2TiCl_2] with *n*-butyllithium in the presence of an excess of cyclooctatetraene. More details on this preparation and characterization are provided as Supplementary Information (SI). To improve accuracy, single-crystal X-ray data were collected at 100 K for the first time. Interestingly, contrary to a previous report of a destructive phase transition below 200 K,[10] the molecular and crystal structures solved for **1** did not differ significantly from those investigated at higher temperatures (Table S4). Dispersion in a diamagnetic crystalline matrix was attempted by co-crystallizing **1** with [CpTi(cht)] (**2,** cht = η^7-$C_7H_7^{3-}$, left of Fig.1) in nominal 1:30 molar proportion (*ca.* 3 mol%). Complex **2** was synthesized following a procedure similar to that employed for **1**; FTIR, elemental analysis, and crystal structure compare well with previous reports.[11]

Variable-temperature X-band ($\nu \approx 9.5$ GHz) CW-EPR spectra of **1** dissolved in toluene (1.0 mmol L^{-1}) are shown in Figure 2 (left). Q-band ($\nu \approx 33.8$ GHz) CW and echo-detected field-swept (EDFS) EPR spectra of **1** in deuterated toluene at 5 K (0.5 mmol L^{-1}) are reported in Figure 2 (right). The low-temperature fully frozen spectra and the powder EPR spectrum of **1** diluted in **2** (Fig. S6) confirm previous reports of an axially anisotropic S=1/2 species with $g_{//} \approx g_e > g_\perp$. This observation indicates that the SOMO has the main contribution from the non-bonding d_{z^2} metal orbital.

The main resonance lines in Fig. S5 and S6 are flanked by the weak hyperfine components due to the two stable, $I \neq 0$ titanium isotopes (^{47}Ti, I=5/2, and ^{49}Ti, I=7/2, natural abundances of 7.44 % and 5.41 % respectively). ^{1}H super-hyperfine structures are only visible at intermediate temperatures (250-180 K) when the tumbling of the molecules averages the anisotropic components. At room temperature, this super-hyperfine structure is partially lost due to line broadening (see Fig. 2 and Fig. S4).

Simulation of the EPR spectra over the whole temperature range was performed by considering a temperature-dependent correlation time in the intermediate regime (more details in SI).[12] The values of the spin Hamiltonian (SH) parameters are reported in Table 1 and compare well with previous reports[8,9b], including detailed ENDOR investigations.[9a]

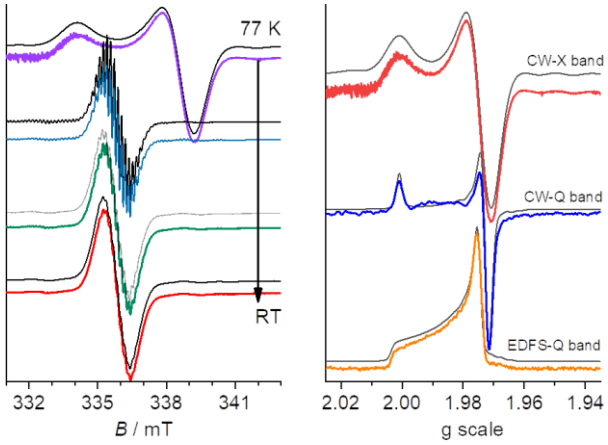

Figure 2. Field-swept EPR spectra of toluene solutions of **1**. Left: X-band CW-EPR spectra between 77 K and RT. Right: Frozen solution spectra at T = 4.5 K and different frequencies, plotted on g-scale to ease comparison. In all cases, simulations are presented as thin black lines (see text and SI for details).

Table 1. Spin Hamiltonian parameters extracted from EPR spectra compared with computed data assuming the X-ray molecular structure and optimizing the structure in the presence of toluene as implicit solvent. Hyperfine and quadrupolar couplings are given in MHz.

	Exp. [a]	Exp.[b]	$\mathbf{1}_{\text{x-ray}}$	$\mathbf{1}_{\text{solv}}$[c]
g_x	1.972(3)	1.972(3)	1.972	1.971
g_y	1.972(3)	1.972(3)	1.973	1.972
g_z	2.001(1)	2.000(8)	2.002	2.002
A_{iso}(^{1}H-Cp)	4.1(3)	4.09	+2.7	+3.4
A_{iso}(^{1}H-cot)	8.8(3)	8.78	+6.2	+7.4
A_x(^{47}Ti)	52.4(8)	52.60(5) [e]	+52	+53.8
A_y(^{47}Ti)	52.4(8)	52.60(5) [e]	+53	+54.1
A_z(^{47}Ti)	*ca.* 5	*ca.* 10	-2.6	-0.6
$P_{//}$(^{47}Ti)[f]	-	*-2.30(2)*	-1.81	-
$P_{//}$(^{49}Ti)[f]	-	*-0.90(2)*	-0.71	-

[a] This work. [b] From ENDOR studies.[9a] [c] The solvent was considered by CPCM model. [d] Values for ^{49}Ti can be obtained by appropriate rescaling. See SI for more details. [e] Average value (^{47}Ti, 52.80; ^{49}Ti, 52.40 MHz). [f] $H_{QS}=P_{//}[I_z^2-⅓(I+1)]$.

As a first necessary step for rationalizing the spin dynamics in [CpTi(cot)], we calculated the static SH parameters using ORCA 4.0 quantum chemistry package.[13] Density Functional Theory (DFT) calculations of the electronic structure with B2PLYP[14] double hybrid functional were performed on three different geometries of the discrete molecule: i) the X-ray structure ($\mathbf{1}_{\text{x-ray}}$), ii) the optimized geometry in the vacuum ($\mathbf{1}_{\text{vac}}$), and iii) the optimized geometry in the presence of implicit toluene solvent modeled by the Conductor-like Polarizable Continuum Model (CPCM)[15] ($\mathbf{1}_{\text{solv}}$). More details are available in SI.

Structural results obtained for $\mathbf{1}_{\text{vac}}$ are in excellent agreement with the experimental findings (Table S7). Similar geometric parameters are calculated for $\mathbf{1}_{\text{solv}}$, in which case the energy barrier for the rotation of the two rings around the z-axis, estimated by rigidly rotating the Cp ring, is found to be very small, *ca.* 40 meV (350 cm^{-1}).

The electronic structure of [CpTi(cot)] in $\mathbf{1}_{\text{xray}}$, $\mathbf{1}_{\text{vac}}$, and $\mathbf{1}_{\text{solv}}$ (right of Figure 1 for $\mathbf{1}_{\text{solv}}$, and Fig. S18-19 for comparison) is characterized by the splitting of the d orbitals in three sets: non-bonding, bonding, and anti-bonding. The latter two arise from the interaction of metal d orbitals with the π systems of the rings. If we take the energy of the d_{z^2} SOMO as reference, the two

bonding sets lie at -0.8 (d_{xz}/d_{yz}) and 0.3 (d_{xy}/d_{x2-y2}) eV respectively, while the antibonding sets lie at 7.9 (d_{xy}/d_{x2-y2}) eV and 9.0 eV(d_{xz}/d_{yz}). The complete non-bonding character of d_z^2 originates from the energy mismatch with the symmetry-adapted fully bonding π orbitals of the ligands.

Interestingly, in [CpTi(cot)] the d_{xz} and d_{yz} orbitals (e_1; $C_{\infty v}$ approximation) interact selectively with the Cp ring, while the d_{xy} and d_{x2-y2} (e_2) orbitals show selective overlap with the cot π system (see Fig. 1 right). Similar behavior was also reported for [CpM(cht)] complexes, M = Cr, V, Ti.[16] The electric dipole moment for **1** is computed to be 0.98 D.

The DFT-calculated SH parameters for $\mathbf{1}_{vac}$ and $\mathbf{1}_{solv}$ are also gathered in Table 1. The agreement with experimental data is again excellent and proves the reliability of the computational protocol. The discrepancy between the experimental and calculated values for $A_z(^{47}Ti)$ has to be considered in the light of the large uncertainty on the experimental values.[9a] More subtle details, such as the anisotropic contributions to the ^1H hyperfine interaction, are also well reproduced (Table S11-12). A small but not negligible σ interaction between the d_z^2 and in-phase π cot and Cp orbitals asymmetrically delocalized on the hydrogen atoms is responsible for the computed ^1H Fermi contact contribution.

Hahn-echo decay experiments were performed in solution to investigate the coherence time of **1**. Deuterated toluene was employed to reduce the solvent contribution to decoherence. The phase memory times, T_m, extracted from the simulation of the decay traces (Fig. S9) provide consistent behavior either using a stretched exponential or a bi-exponential decay. Long T_m values, above 10 μs, are observed below 20 K as shown in Figure 3 (solid squares). Though not comparable to the record coherence times of vanadium(IV) complexes in nuclear spin-free environment,[17] **1** has a remarkably robust coherence for a hydrogen-rich molecule, exceeding or comparable to those observed for complexes with nuclear spin-free ligands in frozen[18] or solid solutions,[19] as well as for endohedral metallofullerenes.[20]

Nutation experiments were carried out at 80 K (inset of Fig. 3), and Rabi oscillation frequencies were found to scale linearly with the microwave magnetic field (Fig. S10), indicating that coherent spin manipulation is feasible.

The observation of a moderate detrimental effect of hydrogen nuclear spins on T_m is not unexpected and indeed was one of the motivations of our study. It is well known that an important contribution to decoherence, namely nuclear spin diffusion, has a non-monotonous dependence on the distance between the magnetic nucleus and the electronic spin. Indeed, the Ti–H distances of *ca.* 3 Å in **1** fall well inside the spin diffusion barrier involving ^1H nuclei.[21] This barrier was theoretically predicted around 4 Å and experimentally found in the 4-6 Å range for other molecular S=1/2 systems.[22] Their contribution to decoherence is therefore limited, although the rotation of the rings is not fully hindered. To verify this hypothesis, we also investigated the spin dynamics of nominal 2% and 3% solid solutions of **1** in **2** by pulsed EPR (see Fig. S11). The extracted characteristic times are reported in Figure 3 (black-and-white squares) and evidence a striking and virtually temperature-independent decrease in T_m to 0.1 μs. This suggests that the hydrogen nuclear spins of neighboring diamagnetic molecules of **2** are very efficient in inducing decoherence. Fast relaxing triplet states, identified through 2D Transient-EPR nutation experiments[23] (Fig. S12-13) and most likely explained by a non-ideal dispersion of **1** in **2,** might also contribute to shortening the coherence lifetime.

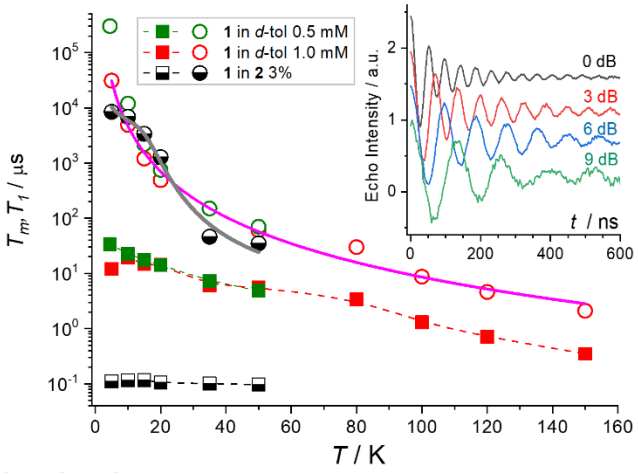

Figure 3. Temperature dependence of T_1 (circles) and T_m (squares) extracted from Q-band pulsed-EPR experiments performed for deuterated toluene frozen solutions of **1** at two concentrations, and for a solid solution of **1** in **2**. The solid lines represent the best-fit curves reproducing T_1 (see text). Broken lines are only a guide to the eye. The inset presents the normalized echo intensity in nutation experiments for the 0.5 mmol L^{-1} solution of **1** at T=80 K.

We then computed T_m for the deuterated frozen solution assuming that instantaneous diffusion dominates (see SI).[24] The resulting value of 59 μs agrees well with the experiment (Figure 3), thus confirming the nature of the main contribution to decoherence in **1**. In fact, hydrogen nuclei in metallocene systems appear to be placed at a distance short enough to minimize spin diffusion but not too close to enhance instantaneous diffusion. Similar favorable conditions have been suggested to justify the relatively long T_m (*ca.* 3 μs) observed in organometallic complexes of yttrium(II).[25]

Spin-lattice relaxation rates were also investigated by pulsed EPR, using inversion-recovery experiments, for 1 mmol L^{-1} and 0.5 mmol L^{-1} toluene-d_8 solutions of **1** (temperature ranges of 4.5-150 K and 4.5-50 K respectively). More details are available in the SI. The resulting saturation-recovery traces recorded at the $g_\perp$ resonance field (Fig. S9) were fitted with a standard stretched exponential equation (stretching parameter in the range 0.68 - 0.93), and the extracted T_1 values are reported in Figure 3 (open circles). The difference observed for the two similar concentrations probably depends on slightly different

freezing times that affect the organization of the solvent around the molecules of **1** (vide infra).[9b] It is interesting to notice in Figure 3 that comparable spin-lattice relaxation times (T_1) are observed for frozen and solid solutions of **1**, though with different temperature dependence.

A deeper understanding of the peculiar quantum spin dynamics of this organometallic S=1/2 system requires to investigate in detail its vibrational properties and their influence on the spin dynamics, a point which we tackle in the following, both experimentally and theoretically.

An early report on the vibrational properties of **1** listed two weak IR-active bands at 61 and 143 cm^{-1}, while the first intense band was reported at 377 cm^{-1}.[26] We performed time-domain THz spectroscopy experiments on a polycrystalline sample of **1** dispersed in high-density polyethylene to detect the presence of low energy modes. More experimental details are reported in SI. Figure 4 presents the spectra recorded at two temperatures between 20 and 300 cm^{-1}, while spectra at additional temperatures are available in Figure S16. Early findings were fully confirmed, and no significant absorptions were observed below the one at 75 cm^{-1}, except for an upturn at the lowest accessible frequencies. Figure 4 also shows a small experimental blue-shift on decreasing the temperature, as found for other complexes.[27]

A theoretical analysis at the DFT level of these low-energy vibrational modes was performed on $\mathbf{1}_{vac}$ and $\mathbf{1}_{sol}$ (see SI for more details).[28] Table 2 reports the computed vibration frequencies for the three lowest modes, while the associated displacements vectors are shown in Figure 4. Noticeable is the extremely small value of the ring rotation frequency for the molecule in vacuum (8 cm^{-1}), in agreement with the calculated small energy barrier preventing free rotation. The inclusion of the solvent has a dramatic effect on this vibration, whose frequency almost triples. The two quasi-degenerate modes just above 100 cm^{-1} were found to correspond to two orthogonal ring-metal-ring bending motions (see Figure 4) and are weakly sensitive to the environment. These results support a previous tentative assignment of the Terahertz spectra.[26]

In order to generate a more comprehensive description, the vibrational spectrum was also computed for the crystalline phase of **1** at the Γ point ($\mathbf{1}_{bulk}$) within a periodic DFT approach (see SI for details).[27b,28-29] The spectrum compares well with the THz data, as shown in Figure 4 where the nature of the lowest vibration modes is also depicted. Interestingly, absorptions up to 75 cm^{-1} are due to linear combinations of Cp and cot ring rotations of different molecules within the unit cell (see Table S8). A group of ring bending modes is computed in the energy range 110-125 cm^{-1}, similar to $\mathbf{1}_{vac}$ and $\mathbf{1}_{solv}$, whereas their relative breathing and out-of-plane C-H bending modes are found above 200 cm^{-1} (see Figure S20 for the displacement vectors associated to these modes).

The spin-vibrational coupling was then calculated for the low energy vibrations to correlate vibrational properties with spin dynamics. Given that the spin dynamics was experimentally investigated at a moderately high magnetic field (1.2 T), and the most abundant Ti isotopes have I=0, modulation of the **g** components is expected to prevail over hyperfine interactions in promoting spin-lattice relaxation. We evaluated the effect of the geometric distortions induced by each vibration on the molecular **g** tensor using state-of-the-art methodologies.[1a,27b,28,30] Briefly, the molecule was distorted along each normal mode, the nine components of the **g** tensor were computed, and their variation fitted with a quadratic polynomial function. Finally, the squares of the nine linear term coefficients were summed up to give the relative spin-vibrational coupling coefficients reported in Table 2.

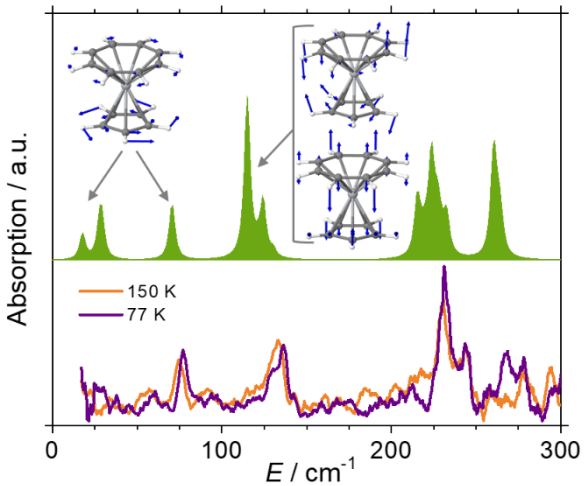

Figure 4. Bottom, experimental absorption of THz radiation by microcrystals of **1** dispersed in high-density polyethylene at two temperatures. Top, calculated spectrum in the crystalline phase, $\mathbf{1}_{bulk}$. Displacement vectors computed for the lowest-energy normal vibrational modes are also shown.

In both the isolated ($\mathbf{1}_{vac}$) and solvated ($\mathbf{1}_{solv}$) molecules, the two vibrations above 100 cm^{-1} are computed to be 4-8 times more efficient in the relaxation process than the low-energy ring rotation mode. This finding agrees with the fact that the SOMO is a d_{z^2} orbital, and its interaction with the π systems is not affected by the lowest vibration due to its symmetry.

Table 2. Computed frequencies (cm^{-1}) and spin-phonon coupling coefficients for the three lowest-energy vibration modes in **1**, assuming a molecule in the vacuum, $\mathbf{1}_{vac}$, or in the presence of implicit toluene, $\mathbf{1}_{solv}$.

Vibration mode	$\mathbf{1}_{vac}$		$\mathbf{1}_{solv}$	
	Freq.	Sp-Ph Coupl	Freq.	Sp-Ph Coupl
1	8	$1.3x10^{-8}$	22	$7.8x10^{-9}$
2	107	$6.4x10^{-8}$	111	$5.3x10^{-8}$
3	111	$4.3x10^{-8}$	115	$4.5x10^{-8}$

It is interesting to correlate our vibrational analysis with the temperature dependence of T_1 reported in Figure 3. Usually, a power law of the type $T_1^{-1} = aT + bT^n$ is employed, with the first term corresponding to the direct process and the second to a two-phonon Raman-like relaxation mechanism. A good simulation (solid purple line in Fig. S15) was obtained considering only the second term, pointing to a negligible influence of the direct mechanism. The best-fit exponent n=2.7(1) is in line with those often encountered in molecular S=1/2 spin systems, but it does not provide physical insight into the mechanisms determining relaxation.

Assuming that low energy optical vibrations are responsible for the Raman-like process, the following expression has been proposed:[31]

$$T_1^{-1} = aT \quad + b\frac{exp\left(\frac{E_{opt}}{k_BT}\right)}{\left(exp\left(\frac{E_{opt}}{k_BT}\right)-1\right)^2} \qquad (1)$$

where the second term takes into account the contribution of an optical mode of energy E_{opt}, while the pre-exponential factor, b, is related to the spin-phonon coupling.

Using Eq. (1) T_1 data of the frozen solution were best fit using E_{opt} = 33 ± 0.1 cm^{-1}, a value not too far from 22 cm^{-1} computed for the rings rotation mode with the implicit modelling of the solvent. The agreement is satisfactory, considering the high sensitivity of ring rotations to the environment. Interestingly, T_1 at high temperature was better reproduced by including also the contribution of the two bending modes listed in Table 2. No additional parameters were introduced, as the energy of the modes was fixed at the calculated values and the b coefficient rescaled to that of the first mode using the computed spin-phonon couplings. The analysis of the different contributions to T_1, reported in Figure S15, evidences the very negligible weight of the direct process, in agreement with the successful simulation with only one term of the power law.

Passing to the solid solution and employing the same fitting procedure, the E_{opt} of the first mode is found at 56 ± 3 cm^{-1}. The sizeable increase in the energy of the optical mode responsible for spin relaxation is in line with the results of our quantum computation in the crystalline phase with ring rotation modes spanning an energy range between 20 and 70 cm^{-1} (Figure 4 and Table S8). We notice that the contribution of the bending modes above 100 cm^{-1} is negligible in the investigated temperature range that is limited by the collapse of the spin-echo. Also, the direct term was fitted with an exponent significantly different from 1 (n = 0.20 ± 0.03). Deviations from unity are expected but only at very low temperatures.[32] However, they have already been observed for S=1/2 systems in solid solutions.[27a,33]

To conclude, this simple S=1/2 organometallic molecule presents very appealing spin coherence properties despite its large number of hydrogen atoms, as they fall inside the spin diffusion barrier. Further, T_1 of both frozen and solid solutions remains long enough not to affect T_m over a reasonable temperature range. This occurs despite the presence of very low energy vibrations, which might represent a point of weakness in this respect. However, our theoretical analysis indicates that these vibrational modes have relatively weak spin-phonon coupling. Under this respect, [CpTi(cot)] may be seen as an S=1/2 analog of what dysprosium(III) metallocene cations currently represent in the field of SMMs.[1-2]

Looking ahead, the rich chemistry of these simple molecules can also be exploited to achieve better control of the spin dynamics. For instance, the introduction of an interannular link, as in silatrovacenophanes,[34] will inhibit the rotations of the rings, allowing disentangling different contributions to the spin-lattice relaxation.

Finally, although other sublimable molecules with good coherence times are known,[24a,33,35] **1** presents the extra desirable feature of a relatively accessible non-bonding d_z^2 singly-occupied orbital. The approachable exploration of these properties distinguishes [CpTi(cot)] as an ideal candidate to act as a coherent spin sensor at the single-molecule level, similar to what was recently achieved with nickelocene for non-coherent nanoscale magnetic sensing.[4a,4b] Besides, spin control with electric fields can also be envisaged for this acentric and polar molecule,[36] as well as single spin coherent manipulation with a scanning tunnel microscope, as recently achieved for Ti adatoms on MgO.[37]

Acknowledgements

This work has been supported by Italian MIUR (Project PRIN 2015-HYFSRT and Progetto Dipartimenti di Eccellenza 2018-2022, ref B96C1700020008), by the EU Commission through the QuantERA Project SUMO and the FETOPEN project FATMOLS (GA 862893), and by the Brazilian CNPq (Project 308426/2016-9) and CAPES (PROEX and PrInt/CAPES-UFPR, Finance Code 001). The computing resources and the related technical support used for this work have been provided by CRESCO/ENEAGRID High Performance Computing infrastructure[38] and its staff.

Keywords: Titanium • Metallocene complexes • Electron Paramagnetic Resonance • Quantum Coherence • DFT

[1] [1] a) C. A. P. Goodwin, F. Ortu, D. Reta, N. F. Chilton, D. P. Mills, *Nature* **2017**, *548*, 439; b) F.-S. Guo, B. M. Day, Y.-C. Chen, M.-L. Tong, A. Mansikkamäki, R. A. Layfield, *Angew. Chem. Int. Ed.* **2017**, *56*, 11445-11449; c) F.-S. Guo, B. M. Day, Y.-C. Chen, M.-L. Tong, A. Mansikkamäki, R. A. Layfield, *Science* **2018**, *362*, 1400-1403; d) K. Randall McClain, C. A. Gould, K. Chakarawet, S. J. Teat, T. J. Groshens, J. R. Long, B. G. Harvey, *Chem. Sci.* **2018**, *9*, 8492-8503; e) C. A. Gould, K. R. McClain, J. M. Yu, T. J. Groshens, F. Furche, B. G. Harvey, J. R. Long, *J. Am. Chem. Soc.* **2019**, *141*, 12967-12973.

[2] L. Escalera-Moreno, J. J. Baldoví, A. Gaita-Ariño, E. Coronado, *Chem. Sci.* **2020**, *11*, 1593-1598.

[3] M. Ding, A. K. Hickey, M. Pink, J. Telser, D. L. Tierney, M. Amoza, M. Rouzières, T. J. Ozumerzifon, W. A. Hoffert, M. P. Shores, E. Ruiz, R. Clérac, J. M. Smith, *Chem. Eur. J.* **2019**, *25*, 10625-10632.

[4] a) B. Verlhac, N. Bachellier, L. Garnier, M. Ormaza, P. Abufager, R. Robles, M. L. Bocquet, M. Ternes, N. Lorente, L. Limot, *Science* **2019**, *366*, 623-627; b) G. Czap, P. J. Wagner, F. Xue, L. Gu, J. Li, J. Yao, R. Q. Wu, W. Ho, *Science* **2019**, *364*, 670-673; c) M. Ormaza, N. Bachellier, M. N. Faraggi, B. Verlhac, P. Abufager, P. Ohresser, L. Joly, M. Romeo, F. Scheurer, M. L. Bocquet, N. Lorente, L. Limot, *Nano Lett.* **2017**, *17*, 1877-1882.

[5] a) J. Ferrando-Soria, E. M. Pineda, A. Chiesa, A. Fernandez, S. A. Magee, S. Carretta, P. Santini, I. J. Vitorica-Yrezabal, F. Tuna, G. A. Timco, E. J. L. McInnes, R. E. P. Winpenny, *Nat. Commun.* **2016**, *7*, 11377; b) A. Gaita-Ariño, F. Luis, S. Hill, E. Coronado, *Nat. Chem.* **2019**, *11*, 301-309; c) M. Atzori, R. Sessoli, *J. Am. Chem. Soc.* **2019**, *141*, 11339-11352; d) S. von Kugelgen, D. E. Freedman, *Science* **2019**, *366*, 1070; e) M. R. Wasielewski, M. D. E. Forbes, N. L. Frank, K. Kowalski, G. D. Scholes, J. Yuen-Zhou, M. A. Baldo, D. E. Freedman, R. H. Goldsmith, T. Goodson, M. L. Kirk, J. K. McCusker, J. P. Ogilvie, D. A. Shultz, S. Stoll, K. B. Whaley, *Nature Reviews Chemistry* **2020**, *4*, 490–504.

[6] H. O. Van Oven, H. J. de Liefde Meijer, *J. Organomet. Chem.* **1969**, *19*, 373-376.

[7] P. A. Kroon, R. B. Helmholdt, *J. Organomet. Chem.* **1970**, *25*, 451-454.

[8] E. Samuel, G. Labauze, D. Vivien, *J. Chem. Soc., Dalton Trans.* **1979**, 956-961.

[9] a) D. Gourier, E. Samuel, *J. Am. Chem. Soc.* **1987**, *109*, 4571-4578; b) G. Labauze, J. B. Raynor, E. Samuel, *J. Chem. Soc., Dalton Trans.* **1980**, 2425-2427.

[10] K. A. Lyssenko, M. Y. Antipin, S. Y. Ketkov, *Russ. Chem. Bull.* **2001**, *50*, 130-141.

[11] a) H. O. Van Oven, H. J. de Liefde Meijer, *J. Organomet. Chem.* **1970**, *23*, 159-163; b) J. D. Zeinstra, J. L. De Boer, *J. Organomet. Chem.* **1973**, *54*, 207-211.

[12] S. Stoll, A. Schweiger, *J. Magn. Reson.* **2006**, *178*, 42-55.

[13] F. Neese, *WIREs Comput. Mol. Sci.* **2018**, *8*, e1327.

[14] S. Grimme, *J. Chem. Phys.* **2006**, *124*, 034108.

[15] M. Cossi, N. Rega, G. Scalmani, V. Barone, *J. Comput. Chem.* **2003**, *24*, 669-681.

[16] M. L. H. Green, D. K. P. Ng, *Chem. Rev.* **1995**, *95*, 439-473.

[17] J. M. Zadrozny, J. Niklas, O. G. Poluektov, D. E. Freedman, *ACS Cent. Sci.* **2015**, *1*, 488-492.

[18] C. J. Yu, M. J. Graham, J. M. Zadrozny, J. Niklas, M. D. Krzyaniak, M. R. Wasielewski, O. G. Poluektov, D. E. Freedman, *J. Am. Chem. Soc.* **2016**, *138*, 14678-14685.

[19] K. Bader, D. Dengler, S. Lenz, B. Endeward, S.-D. Jiang, P. Neugebauer, J. van Slageren, *Nat. Commun.* **2014**, *5*, 5304.

[20] a) R. B. Zaripov, Y. E. Kandrashkin, K. M. Salikhov, B. Büchner, F. Liu, M. Rosenkranz, A. A. Popov, V. Kataev, *Nanoscale* **2020**; b) Z. Liu, B.-W. Dong, H.-B. Meng, M.-X. Xu, T.-S. Wang, B.-W. Wang, C.-R. Wang, S.-D. Jiang, S. Gao, *Chem. Sci.* **2018**, *9*, 457-462.

[21] E. R. Canarie, S. M. Jahn, S. Stoll, *J. Phys. Chem. Lett.* **2020**, 3396-3400.

[22] a) M. J. Graham, C. J. Yu, M. D. Krzyaniak, M. R. Wasielewski, D. E. Freedman, *J. Am. Chem. Soc.* **2017**, *139*, 3196-3201; b) J. Chen, C. Hu, J. F. Stanton, S. Hill, H.-P. Cheng, X.-G. Zhang, *J. Phys. Chem. Lett.* **2020**, *11*, 2074-2078.

[23] S. Stoll, G. Jeschke, M. Willer, A. Schweiger, *J. Magn. Reson.* **1998**, *130*, 86-96.

[24] a) M. Warner, S. Din, I. S. Tupitsyn, G. W. Morley, A. M. Stoneham, J. A. Gardener, Z. Wu, A. J. Fisher, S. Heutz, C. W. M. Kay, G. Aeppli, *Nature* **2013**, *503*, 504-508; b) L. Escalera-Moreno, A. Gaita-Ariño, E. Coronado, *Phys. Rev. B* **2019**, *100*, 064405.

[25] A. M. Ariciu, D. H. Woen, D. N. Huh, L. E. Nodaraki, A. K. Kostopoulos, C. A. P. Goodwin, N. F. Chilton, E. J. L. McInnes, R. E. P. Winpenny, W. J. Evans, F. Tuna, *Nat. Commun.* **2019**, *10*, 3330.

[26] J. Goffart, L. Hockst, *Spectrochim. Acta, Pt. A: Mol. Spectrosc.* **1981**, *37*, 609-614.

[27] a) T. Yamabayashi, M. Atzori, L. Tesi, G. Cosquer, F. Santanni, M.-E. Boulon, E. Morra, S. Benci, R. Torre, M. Chiesa, L. Sorace, R. Sessoli, M. Yamashita, *J. Am. Chem. Soc.* **2018**, *140*, 12090-12101; b) A. Albino, S. Benci, L. Tesi, M. Atzori, R. Torre, S. Sanvito, R. Sessoli, A. Lunghi, *Inorg. Chem.* **2019**, *58*, 10260-10268.

[28] A. Lunghi, F. Totti, S. Sanvito, R. Sessoli, *Chem. Sci.* **2017**, *8*, 6051-6059.

[29] E. Garlatti, L. Tesi, A. Lunghi, M. Atzori, D. J. Voneshen, P. Santini, S. Sanvito, T. Guidi, R. Sessoli, S. Carretta, *Nat. Commun.* **2020**, *11*, 1751.

[30] a) L. Escalera-Moreno, N. Suaud, A. Gaita-Ariño, E. Coronado, *J. Phys. Chem. Lett.* **2017**, *8*, 1695-1700; b) R. Mirzoyan, R. G. Hadt, *Phys. Chem. Chem. Phys.* **2020**, *22*, 11249-11265

[31] a) S. S. Eaton, J. Harbridge, G. A. Rinard, G. R. Eaton, R. T. Weber, *Appl. Magn. Reson.* **2001**, *20*, 151-157; b) A. Lunghi, S. Sanvito, *J. Phys. Chem. Lett.* **2020**, *11*, 6273-6278.

[32] A. Lunghi, S. Sanvito, *Science Advances* **2019**, *5*, eaax7163.

[33] M. Atzori, L. Tesi, E. Morra, M. Chiesa, L. Sorace, R. Sessoli, *J. Am. Chem. Soc.* **2016**, *138*, 2154-2157.

[34] C. Elschenbroich, F. Paganelli, M. Nowotny, B. Neumüller, O. Burghaus, *Z. Anorg. Allg. Chem.* **2004**, *630*, 1599-1606.

[35] a) K. Bader, M. Winkler, J. van Slageren, *Chem. Commun.* **2016**, *52*, 3623-3626; b) S. Lenz, K. Bader, H. Bamberger, J. van Slageren, *Chem. Commun.* **2017**, *53*, 4477-4480.

[36] a) J. J. Liu, J. Mrozek, W. K. Myers, G. A. Timco, R. E. P. Winpenny, B. Kintzel, W. Plass, A. Ardavan, *Phys. Rev. Lett.* **2019**, *122*, 037202; b) Z. Liu, Y.-X. Wang, Y.-H. Fang, S.-X. Qin, Z.-M. Wang, S.-D. Jiang, S. Gao, *Nat. Sci. Rev.* **2020**, in press (https://doi.org/10.1093/nsr/nwaa148); c) J.
J. Liu, J. Mrozek, Y. Duan, A. Ullah, J. J. Baldoví, E. Coronado, A. Gaita-Ariño, A. Ardavan, preprint https://arxiv.org/abs/2005.01029

[37] K. Yang, W. Paul, S. H. Phark, P. Willke, Y. Bae, T. Choi, T. Esat, A. Ardavan, A. J. Heinrich, C. P. Lutz, *Science* **2019**, *366*, 509-512.

[38] G. Ponti, e. al., in *International Conference on High Performance Computing and Simulation, HPCS 2014, Vol. art. no. 6903807*, **2014**, pp. 1030-1033.